AIAA JOURNAL
Vol. 31, No. 4, April 1993

Vibration and Damping Analysis of Composite Laminates Using Shear Deformable Finite Element

K. N. Koo* and I. Lee†
Korea Advanced Institute of Science and Technology, Taejon, Republic of Korea

The effects of transverse shear deformation on the modal loss factors as well as the natural frequencies of composite laminated plates have been studied using the finite element method based on the shear deformable plate theory. The complex modulus of an orthotropic lamina is employed to model damping effect, and a modal approach to the resultant complex eigenvalue problem is introduced to save a considerable amount of computation time. The present result gives a good agreement with the solution of the modal strain energy (MSE) method. The damping is very high when the composite laminated plates are subject to large transverse shear deformation as well as in-plane shear deformation.

Nomenclature

A_{ij} = transverse shear stiffness
a, b = lengths of plate in x and y directions, respectively
D_{ij} = bending stiffness
E, G = elastic moduli
h = thickness of laminate
i = $\sqrt{-1}$
K, M = stiffness and mass matrices, respectively
M, Q = resultant moment and shear force, respectively
$\bar{Q}_{ij}$ = reduced stiffness
q = generalized eigenvector
t = thickness of lamina
u, v, w = displacements in x, y, and z directions, respectively
V_f = fiber volume fraction
γ = loss angle
ϵ, σ = strain and stress, respectively
ζ = damping ratio
η = loss factor
θ = fiber orientation
λ = eigenvalue
ρ = mass density of laminate
Φ = modal matrix
ϕ = rotation of the transverse normal
Ψ = specific damping capacity
ψ = shape function
ω = angular frequency

Subscripts
0 = value for midplane
1, 2, 3 = principal axis of lamina
x, y, z = reference of axis of laminate
, = operator for partial differentiation

Superscripts
R, I = real and imaginary parts of complex value, respectively
T = operator of transpose of matrix
* = complex value

Received March 10, 1992; revision received July 31, 1992; accepted for publication July 31, 1992.

*Graduate Research Assistant, Department of Aerospace Engineering.
†Associate Professor, Department of Aerospace Engineering. Member AIAA.

Introduction

THE damping in composite materials plays an important role in controlling the resonant response of aerospace structures and thus in prolonging their service life under repeated loading or impact.[1] Fiber-reinforced composites, in general, have a higher damping than metals. However, their value depends on fiber and resin types, fiber orientation, and stacking sequence.[2]

Research on the damping analysis of composites is not so extensive as that on the undamped free vibration analysis. Gibson and Plunkett[3] reviewed experimental and analytical efforts to characterize the dynamic properties of fiber-reinforced composite materials. Lin et al.[4] used a damped element model based on the modal strain energy (MSE) method to predict the specific damping capacity (SDC) of composite laminated plates. Recently, Bicos and Springer[5] introduced the damped element model into a shell structure. Hashin[6] applied the elastic-viscoelastic correspondence principle to relate the elastic moduli and creep compliances of the viscoelastic composites. Alam and Asnani[7] used the concept of the complex modulus for the vibration and damping analysis for composite plates and shells by series solution. The complex modulus, which consists of a real part representing elastic stiffness and an imaginary part representing dissipation, has been widely used to model the behavior of linear viscoelastic materials under sinusoidal vibration. Also, Malhotra et al.[8] studied damping characteristics of orthotropic triangular plates by using the complex moduli and three-noded triangular finite elements based on the classical plate theory.

In this paper, the complex eigenvalue problem based on complex moduli is formulated by using a shear deformable finite element method. Because the complex eigenvalue problem with complex stiffness matrix needs a large amount of computation time, many researchers have preferred the MSE method in which both strain energy and dissipated energy are obtained from undamped mode shape. However, that disadvantage can be overcome by using a modal approach. As an alternative method to the MSE method, the modal approach to damping analysis of composite laminated plates is introduced to save a considerable amount of computation time by reducing the large degrees of freedom of the complex eigenvalue problem. The modal approach gives more accurate results than the MSE method, especially for high damping problems. Although the transverse shear effect was considered on the undamped free vibration in many papers, it is not so easy to find that effect on the damping characteristics. In this paper, the shear deformable plate theory is applied to the vibration and damping analysis of fiber-reinforced composite laminates to see the transverse shear effect. The developed

computer program can predict the natural frequencies, the modal loss factors, and the complex modal vectors.

Theory

Complex Modulus of Lamina

Damping is a quality inherent in all known materials and affects the dynamic response greatly near the resonant frequency. The damping of given structures has different sources.[9] First, and our concern, is the "material damping," which is present in any material and is the minimum level that total damping can achieve. Next is the "structural damping," which occurs when two or more neighboring components of structure rub against each other while vibrating. A third mechanism is the "viscous damping," where dissipation occurs by motion within a fluid.

Definitions of damping are varied according to testing method, and their relationship is as follows:

$$\eta = \frac{\Psi}{2\pi} = \frac{E^I}{E^R} = \tan\gamma = 2\zeta = \frac{\omega_2^2 - \omega_1^2}{2\omega_n^2} \tag{1}$$

According to the elastic-viscoelastic correspondence principle, the complex moduli of an orthotropic material are defined as follows:

$$E_1^* = E_1(1 + i\,\eta_1), \qquad E_2^* = E_2(1 + i\,\eta_2)$$

$$G_{12}^* = G_{12}(1 + i\,\eta_{12}), \qquad G_{13}^* = G_{13}(1 + i\,\eta_{13}) \tag{2}$$

$$G_{23}^* = G_{23}(1 + i\,\eta_{23})$$

The constitutive relations in x-y coordinates (Fig. 1) for the k^{th} layer become

$$\begin{Bmatrix}\sigma_x\\ \sigma_y\\ \tau_{xy}\end{Bmatrix}_k = \begin{bmatrix}\bar{Q}_{11}^* & \bar{Q}_{12}^* & \bar{Q}_{16}^*\\ \bar{Q}_{12}^* & \bar{Q}_{22}^* & \bar{Q}_{26}^*\\ \bar{Q}_{16}^* & \bar{Q}_{26}^* & \bar{Q}_{66}^*\end{bmatrix}_k \begin{Bmatrix}\epsilon_x\\ \epsilon_y\\ \gamma_{xy}\end{Bmatrix}_k$$

$$\begin{Bmatrix}\tau_{yz}\\ \tau_{zx}\end{Bmatrix}_k = \begin{bmatrix}\bar{Q}_{44}^* & \bar{Q}_{45}^*\\ \bar{Q}_{45}^* & \bar{Q}_{55}^*\end{bmatrix}_k \begin{Bmatrix}\gamma_{yz}\\ \gamma_{zx}\end{Bmatrix}_k \tag{3}$$

Finite Element Formulation

The transverse shear deformation of a vibrating plate becomes more important when the length-to-thickness ratio decreases and when the mode number and the ratio of the extensional modulus to the shear modulus increase. Another advantage of the shear deformable plate theory is the simplicity in formulating a finite element model because this theory requires only C^0 elements. Using the plate theory developed by Yang et al.[10] which is the extension of the Mindlin plate theory to anisotropic plates, the displacements are assumed to be of the form

$$u(x, y, z, t) = u_0(x, y, t) + z\phi_x(x, y, t)$$

$$v(x, y, z, t) = v_0(x, y, t) + z\phi_y(x, y, t) \tag{4}$$

$$w(x, y, t) = w(x, y, t)$$

where t is the time.

The resultant forces and moments are obtained by integrating the stresses, given in Eq. (3), through the laminate thickness. For the symmetric laminates, we have

$$\begin{Bmatrix}M_x\\ M_y\\ M_{xy}\end{Bmatrix} = \begin{bmatrix}D_{11}^* & D_{12}^* & D_{16}^*\\ D_{12}^* & D_{22}^* & D_{26}^*\\ D_{16}^* & D_{26}^* & D_{66}^*\end{bmatrix} \begin{Bmatrix}\phi_{x,x}\\ \phi_{y,y}\\ \phi_{x,y} + \phi_{y,x}\end{Bmatrix}$$

$$\begin{Bmatrix}Q_y\\ Q_x\end{Bmatrix} = \begin{bmatrix}A_{44}^* & A_{45}^*\\ A_{45}^* & A_{55}^*\end{bmatrix} \begin{Bmatrix}w_{,y} + \phi_y\\ w_{,x} + \phi_x\end{Bmatrix} \tag{5}$$

The assumption for the shear deformation, Eq. (4), gives constant shear distribution through the plate thickness. Therefore, for the more accurate estimation of shear forces, the transverse shear stiffness A_{ij}^* is determined from the assumption that the transverse shear stresses are distributed parabolically across the laminated thickness[11]:

$$A_{ij}^* = \frac{5}{4}\sum_{k=1}^{N} (\bar{Q}_{ij}^*)_k \left[(z_k - z_{k-1}) - \frac{4}{3h^2}(z_k^3 - z_{k-1}^3)\right] \qquad i, j = 4, 5 \tag{6}$$

The equations of motion in terms of moment and transverse shear resultants, neglecting body forces and transverse load, are obtained by integrating the equilibrium equations:

$$\frac{\partial Q_x}{\partial x} + \frac{\partial Q_y}{\partial y} = P\frac{\partial^2 w}{\partial t^2} \tag{7a}$$

$$\frac{\partial M_x}{\partial x} + \frac{\partial M_{xy}}{\partial y} - Q_x = I\frac{\partial^2 \phi_x}{\partial t^2} \tag{7b}$$

$$\frac{\partial M_{xy}}{\partial x} + \frac{\partial M_y}{\partial y} - Q_y = I\frac{\partial^2 \phi_y}{\partial t^2} \tag{7c}$$

where P and I are defined as

$$(P, I) = \int_{-\frac{h}{2}}^{\frac{h}{2}} (1, z^2)\,\rho\,dz \tag{8}$$

The governing equation can be obtained by substituting Eq. (5) into Eq. (7) and assuming sinusoidal oscillation with respect to time:

$$[A_{45}^*(w_{,y} + \phi_y) + A_{55}^*(w_{,x} + \phi_x)]_{,x} + [A_{44}^*(w_{,y} + \phi_y) + A_{45}^*(w_{,x} + \phi_x)]_{,y} = -\lambda^* P w \tag{9a}$$

$$[D_{11}^*\phi_{x,x} + D_{12}^*\phi_{y,y} + D_{16}^*(\phi_{x,y} + \phi_{y,x})]_{,x} + [D_{16}^*\phi_{x,x} + D_{26}^*\phi_{y,y} + D_{66}^*(\phi_{x,y} + \phi_{y,x})]_{,y} - A_{45}^*(w_{,y} + \phi_y) - A_{55}^*(w_{,x} + \phi_x) = -\lambda^* I\,\phi_x \tag{9b}$$

$$[D_{16}^*\phi_{x,x} + D_{26}^*\phi_{y,y}^* + D_{66}^*(\phi_{x,y} + \phi_{y,x})]_{,x} + [D_{12}^*\phi_{x,x} + D_{22}^*\phi_{y,y} + D_{26}^*(\phi_{x,y} + \phi_{y,x})]_{,y} - A_{44}^*(w_{,y} + \phi_y) - A_{45}^*(w_{,x} + \phi_x) = -\lambda^* I\,\phi_y \tag{9c}$$

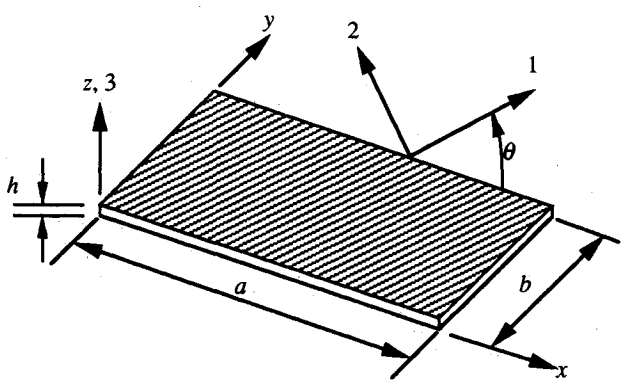

Fig. 1 Coordinate systems of geometric axes and principal material axes.

The midplane Ω of the plate is subdivided into a finite number of elements $\Omega_e (e = 1, 2, \ldots)$. Over each element Ω_e, the displacements are interpolated by expressions of the form

$$w = \sum_{i=1}^{n} w_i \psi_i \qquad \phi_x = \sum_{i=1}^{n} \phi_{x_i} \psi_i \qquad \phi_y = \sum_{i=1}^{n} \phi_{y_i} \psi_i \tag{10}$$

where the various ψ_i are the interpolation functions, and n is the number of nodes per element. With the use of Eq. (10) and ψ_i as weighting function, the finite element equations can be obtained by applying the weighted residual method to Eq. (9):

$$\begin{pmatrix} [K^{*11}] & [K^{*12}] & [K^{*13}] \\ & [K^{*22}] & [K^{*23}] \\ & & [K^{*33}] \end{pmatrix} \begin{Bmatrix} \{w\} \\ \{\phi_x\} \\ \{\phi_y\} \end{Bmatrix} - \lambda^* \begin{pmatrix} [M^{11}] & [0] & [0] \\ & [M^{22}] & [0] \\ & & [M^{33}] \end{pmatrix} \begin{Bmatrix} \{w\} \\ \{\phi_x\} \\ \{\phi_y\} \end{Bmatrix} = \begin{Bmatrix} \{0\} \\ \{0\} \\ \{0\} \end{Bmatrix} \tag{11}$$

where the element stiffness and mass matrices are

$$K_{ij}^{*11} = \int_{\Omega_e} \left[A_{45}^* \left(\frac{\partial \psi_j}{\partial y} \frac{\partial \psi_i}{\partial x} + \frac{\partial \psi_j}{\partial x} \frac{\partial \psi_i}{\partial y} \right) + A_{55}^* \frac{\partial \psi_j}{\partial x} \frac{\partial \psi_i}{\partial x} + A_{44}^* \frac{\partial \psi_j}{\partial x} \frac{\partial \psi_i}{\partial x} \right] dx\, dy$$

$$K_{ij}^{*12} = \int_{\Omega_e} \left(A_{55}^* \psi_j \frac{\partial \psi_j}{\partial x} + A_{45}^* \psi_j \frac{\partial \psi_i}{\partial x} \right) dx\, dy$$

$$K_{ij}^{*13} = \int_{\Omega_e} \left(A_{45}^* \psi_j \frac{\partial \psi_i}{\partial x} + A_{44}^* \psi_j \frac{\partial \psi_i}{\partial x} \right) dx\, dy$$

$$K_{ij}^{*22} = \int_{\Omega_e} \left[D_{11}^* \frac{\partial \psi_j}{\partial x} \frac{\partial \psi_i}{\partial x} + D_{16}^* \left(\frac{\partial \psi_j}{\partial y} \frac{\partial \psi_i}{\partial x} + \frac{\partial \psi_j}{\partial x} \frac{\partial \psi_i}{\partial y} \right) + D_{66}^* \frac{\partial \psi_j}{\partial y} \frac{\partial \psi_i}{\partial y} + A_{55}^* \psi_j \psi_i \right] dx\, dy$$

$$K_{ij}^{*23} = \int_{\Omega_e} \left(D_{12}^* \frac{\partial \psi_j}{\partial y} \frac{\partial \psi_i}{\partial x} + D_{16}^* \frac{\partial \psi_j}{\partial x} \frac{\partial \psi_i}{\partial x} + D_{26}^* \frac{\partial \psi_j}{\partial y} \frac{\partial \psi_i}{\partial y} + D_{66}^* \frac{\partial \psi_j}{\partial x} \frac{\partial \psi_i}{\partial y} + A_{45}^* \psi_j \psi_i \right) dx\, dy$$

$$K_{ij}^{*33} = \int_{\Omega_e} \left[D_{22}^* \frac{\partial \psi_j}{\partial y} \frac{\partial \psi_i}{\partial y} + D_{26}^* \left(\frac{\partial \psi_j}{\partial y} \frac{\partial \psi_i}{\partial x} + \frac{\partial \psi_j}{\partial x} \frac{\partial \psi_i}{\partial y} \right) + D_{66}^* \frac{\partial \psi_j}{\partial x} \frac{\partial \psi_i}{\partial x} + A_{44}^* \psi_j \psi_i \right] dx\, dy$$

$$M_{ij}^{11} = \int_{\Omega_e} P \psi_i \psi_j \, dx\, dy \qquad M_{ij}^{22} = \int_{\Omega_e} I \psi_i \psi_j \, dx\, dy$$

$$M_{ij}^{33} = \int_{\Omega_e} I \psi_i \psi_j \, dx\, dy \tag{12}$$

The reduced Gauss integration rule is used for the evaluation of the transverse shear terms to avoid the shear locking.[12] Nine-node quadrilateral isoparametric elements are used in this analysis.

Modal Approach

Since Eq. (11) is the complex eigenvalue problem with large degree of freedom (DOF), it requires a large amount of computation time. Therefore, a modal approach is adopted. Equation (11) can be rewritten in the following matrix form:

$$[K^* - \lambda^* M]\, u = 0 \tag{13}$$

Eigenvector u can be transformed into q^* using undamped vibration modes Φ as basis functions for damped analysis:

$$u = \Phi q^* \tag{14}$$

where $\Phi = [\phi_1\ \phi_2\ \phi_3, \ldots, \phi_N]$ in the case to taking N modes. Premultiplying Eq. (13) with Φ^T and substituting Eq. (14) into Eq. (13), we obtain

$$\Phi^T [K^* - \lambda^* M] \Phi\, q^* = 0 \tag{15}$$

As a result, the dimension of Eq. (15) is reduced to $N \times N$. The reduced eigenvalue problem, Eq. (15), gives the natural frequency ω and modal loss factor η for each mode as follows:

$$\omega^2 = \mathrm{Re}[\lambda^*] \qquad \eta = \frac{\mathrm{Im}[\lambda^*]}{\mathrm{Re}[\lambda^*]} \tag{16}$$

where Re[ ] and Im[ ] mean real and imaginary parts, respectively.

Results and Discussion

Comparison with Reported Results

The composite laminates used in this analysis consist of high modulus and strength (HMS) carbon fiber in DX-210 epoxy resin that is given in Table 1. This material was also used by Lin et al.[4] The value for η_{23} was not given in Ref. 4, and the value for η_{23} was taken as the same value as that for η_{12}. The boundary conditions of rectangular composite plates are all free (FFFF). Plate data used for the comparison with the results of Lin et al.[4] are detailed in Table 2. The convergence test results of natural frequencies for plate 762 in Table 2 are given in Fig. 2. The natural frequencies for 5×5 mesh, which are obtained by using the nine-node isoparametric element, are regarded as converged. The loss factors were not much affected by the number of modes chosen for the analysis. In this modal approach, 10 modes excluding rigid-body modes were taken for the computation.

Table 3 shows the comparison between the present results and the results of Lin et al.[4] for the natural frequencies and the modal loss factors. In this case, the plate is very thin. The present results give a good agreement with the results of Lin et al.[4] The modal approach gives good results without loss of accuracy. There is a little difference between the modal approach and the MSE method. The present modal approach gives better results than the MSE method compared with the solution of the original complex eigensystem. Elastic moduli and loss factors for a specified fiber volume fraction in Table 2 are evaluated by the micromechanics theory.[13] In this analysis, a nine-node isoparametric element is used. The mesh size is selected as 5×5. At each node point, we have three degrees of freedom (w, ϕ_x, and ϕ_y). Therefore, if we use the original system, Eq. (13), the matrix dimension of the complex eigenvalue problem is 363×363. Instead of solving the time-consuming complex eigenvalue problem, we solve the reduced eigenvalue problem of which the matrix dimension of 10×10. Therefore, we can save a large amount of computation time by reducing the matrix dimension of the complex eigensystem.

Transverse Shear Effects

To see the transverse shear effects on the natural frequencies and modal loss factors, the following material properties of HMS/DX-210 are used: $\rho = 1566.0$ kg/m^3, $V_f = 0.516$, and $a = b = 200$ mm.

For a simply supported plate (SSSS) and a clamped plate (CCCC), the following boundary conditions are applied, respectively:

1) Simply supported plate (SSSS)
   $w = 0$ at all edges
   $\phi_x(x, 0) = \phi_x(x, b) = 0$
   $\phi_y(0, y) = \phi_y(a, y) = 0$

Table 1 Material properties[4]

Material	E_1, GPa	E_2, GPa	G_{12}, GPa	η_1	η_2	η_{12}	ν_{12}	V_f
HMS/DX-210	172.7	7.2	3.76	7.162×10^{-4}	6.7816×10^{-3}	1.122×10^{-2}	0.3	0.5
DX-210/BF400	3.21	3.21	1.20	1.041×10^{-2}	1.041×10^{-2}	1.064×10^{-2}	0.34	0.0

Table 2 Plate data[4]

Plate No.	No. of layers	Density, kg/m^3	Thickness, mm	$a(=b)$, mm	V_f	Stacking sequence
762	8	1566	1.58	178	0.516	$[0/0/0/0]_s$
764	8	1446	2.12	235	0.342	$[0/90/0/90]_s$
770	8	1551.4	1.62	215	0.494	$[0/90/45/-45]_s$
772	12	1636	2.02	216	0.618	$[0/\mp 60/0/\mp 60]_s$

Table 3 Natural frequencies and modal loss factors for all-free plates

	Natural frequencies, Hz				Modal loss factors, $\times 10^{-2}$				
		Present	Lin et al[4]		Present			Lin et al[4]	
Plate no.	Mode	FEM	FEM	Exp	Modal approach[a]	MSE method	Original system[b]	FEM[c]	Exp
762	1	83.90	83.57	81.5	1.0630	1.0628	1.0694	1.0759	1.1141
	2	111.93	118.42	107.4	0.6418	0.6459	0.6401	0.6821	0.7799
	3	204.19	207.79	196.6	0.9347	0.9341	0.9341	0.9374	0.8594
	4	311.32	329.41	295.5	0.6422	0.6462	0.6426	0.6573	0.7480
	5	405.06	419.83	382.5	0.8123	0.8115	0.8123	0.8133	0.7639
	6	546.70	546.93	531.0	0.0771	0.0797	0.0772	0.0748	——
764	1	53.20	58.10	68.9	1.4773	1.4772	1.4773	1.2414	1.0584
	2	210.21	213.31	218.9	0.1591	0.1603	0.1590	0.1448	0.1671
	3	235.79	243.47	251.2	0.4294	0.4294	0.4295	0.3979	0.4138
	4	300.39	302.51	305.4	0.1033	0.1033	0.1033	0.0955	0.1464
	5	318.47	324.16	323.5	0.2540	0.2540	0.2539	0.2403	0.2706
	6	415.65	441.62	452.5	0.4700	0.4662	0.4700	0.4361	0.4775
770	1	86.78	86.33	77.8	0.4860	0.4895	0.4856	0.4950	0.6525
	2	255.30	224.49	202.7	0.1235	0.1255	0.1235	0.1273	0.1464
	3	280.78	280.42	258.0	0.2659	0.2659	0.2659	0.2706	0.2706
	4	300.10	298.81	298.7	0.0941	0.0933	0.0942	0.0923	0.1225
	5	349.61	348.36	322.0	0.1877	0.1897	0.1876	0.1894	0.1910
	6	510.55	512.24	496.7	0.2853	0.2842	0.2853	0.2881	0.3342
772	1	166.46	165.17	156.6	0.2232	0.2266	0.2231	0.2292	0.2228
	2	276.64	279.14	272.0	0.1353	0.1383	0.1354	0.1480	0.1401
	3	384.63	387.80	372.3	0.0972	0.0957	0.0972	0.1003	0.1035
	4	431.01	432.57	407.8	0.1886	0.1898	0.1886	0.1958	0.2005
	5	511.06	511.14	486.1	0.1517	0.1548	0.1517	0.1560	0.1576
	6	787.74	800.37	779.0	0.1352	0.1342	0.1352	0.1464	——

[a]Ten modes are used in the modal approach.
[b]Matrix dimension of Eq. (13) is 363×363, and stiffness matrix is complex valued.
[c]These results are computed by MSE method.

2) Clamped plate (CCCC)

$w = 0$ at all edges

$\phi_x = \phi_y = 0$ at all edges

Figure 3 shows the nondimensionalized natural frequencies, $\omega a^2(\rho/E_2h^2)^{1/2}$ and modal loss factors, η vs the side-to-thickness ratio, a/h for an all-free $[0/90/0/90]_s$ square plate. Both the natural frequencies and the modal loss factors are greatly affected by the side-to-thickness ratio. The effect of the transverse shear is significant for the thick plate (when the side-to-thickness ratio is less than 20). It is also shown that the higher the mode number, the larger the transverse shear effect.

Figure 4 illustrates the fundamental frequencies and modal loss factors of all-free square plates with three types of stacking sequences: $[0/0/0/0]_s$, $[\pm 45/\pm 45]_s$, and $[0/90/0/90]_s$. The angle-ply $[\pm 45/\pm 45]_s$ plate has the highest natural frequency and the lowest loss factor. The cross-ply $[0/90/0/90]_s$ plate has the highest loss factor. The values of natural frequencies and the loss factors of the $[0/0/0/0]_s$ plate are very close to those of the $[\pm 45/\pm 45]_s$ plate. The transverse shear effects for the three plates become dominant when the side-to-thickness ratio (a/h) is less than 20. The angle-ply $[\pm 45/\pm 45]_s$ plate has the greatest effect of the transverse shear on the natural frequency and the loss factor. Since the fundamental mode shape is torsion and the $[\pm 45/\pm 45]_s$ plate among three plates has the lowest ratio of A_{44} (or A_{55}) to D_{66}, this plate has the greatest effect of the transverse shear.

Figure 5 describes the fundamental frequencies and the modal loss factors of simply supported square plates with three types of stacking sequences: $[0/0/0/0]_s$, $[\pm 45/\pm 45]_s$, and $[0/90/0/90]_s$. These sequences are the same as those given in Fig. 4. The angle-ply $[\pm 45/\pm 45]_s$ plate has the highest natural frequency and the lowest loss factor when $a/h > 15$. The $[0/0/0/0]_s$ and $[0/90/0/90]_s$ plates have almost the same fundamental frequencies and loss factors. The transverse shear effects for the simply supported plates become dominant when a/h is less than 30. This result shows that SSSS plates are "more transverse shear deformable" than FFFF plates because SSSS plates have more constraints at the boundaries compared with FFFF plates.

Figure 6 shows the fundamental frequencies and the modal loss factors of clamped square plates with the same stacking sequences as given in Fig. 4: $[0/0/0/0]_s$, $[\pm 45/\pm 45]_s$, and

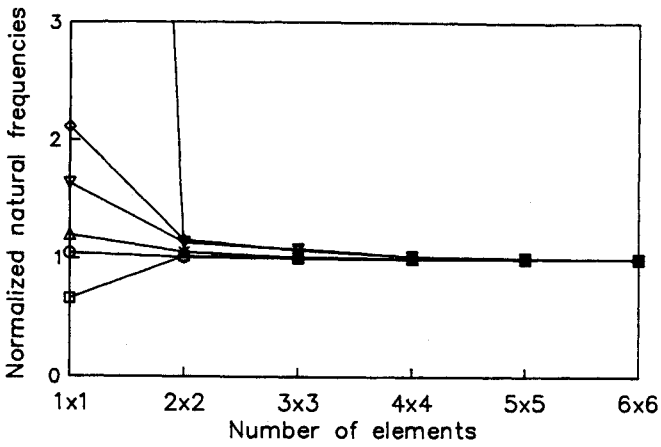

Fig. 2 Convergence of natural frequencies of plate 762 (natural frequencies are normalized by those for 6×6 elements).

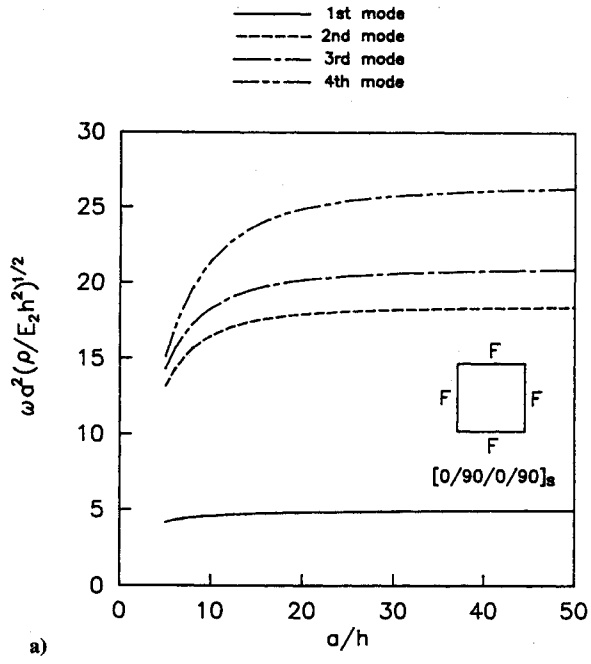

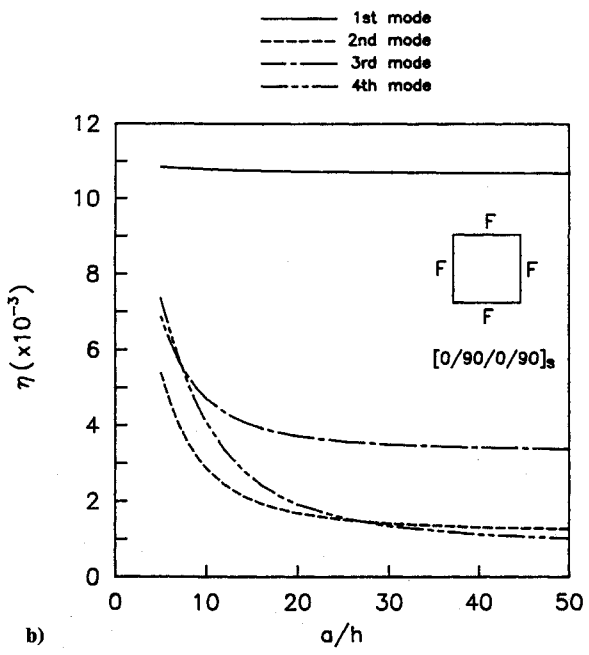

Fig. 3 Dependency of the transverse shear effect on the mode number for all-free (FFFF) $[0/90/0/90]_s$ plate: a) natural frequencies and b) modal loss factors.

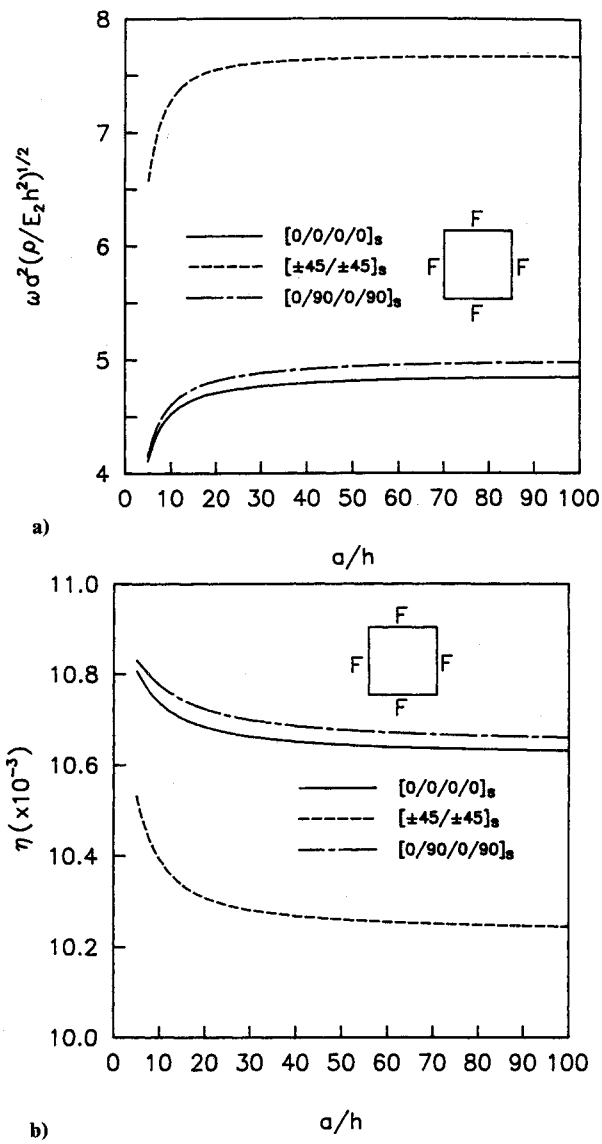

Fig. 4 Fundamental frequencies and loss factors for unidirectional, cross-ply, and angle-ply all-free (FFFF) plate: a) fundamental frequencies and b) fundamental loss factors.

$[0/90/0/90]_s$. The natural frequencies and the loss factors of the three plates are very close. Therefore, the clamped plates have very small influence on the stacking sequence. The transverse shear effects of these plates become dominant when a/h is less than 40. The clamped plate has the greatest transverse shear effect among three types of plate: clamped, simply supported, and free. The transverse shear effect increases as the degree of constraints on the boundary increases.

Effect of Fiber Orientation

To study the effect of the fiber orientation on the natural frequency and the modal loss factor, the material properties given in Table 1 and the plate data for plate 762 given in Table 2 are used except for the stacking sequence of $[0/\pm\theta/90]_s$. The all-free boundary condition is considered.

Figure 7 shows the contour plots of the lowest first four modes for two fiber orientations: $\theta = 0$ and 45 deg of the $[0/\pm\theta/90]_s$ plate. Because the imaginary parts of the mode shape are very small compared with the real parts, only the real parts are plotted in Fig. 7. The lines with the * symbol are nodal lines. The mode shapes are significantly affected by the fiber orientation. When the fiber orientation angle is zero, the first mode is the first torsion, the second mode is the first bending, the third mode is the second torsion, and the fourth mode is the second bending. When the fiber orientation angle

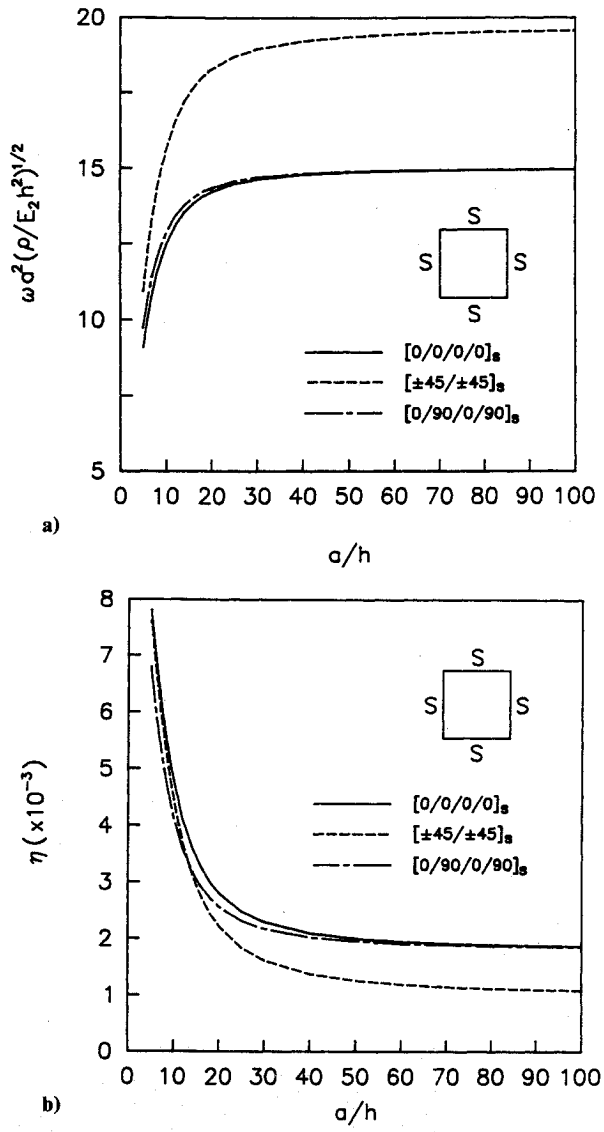

Fig. 5 Fundamental frequencies and loss factors for unidirectional, cross-ply, and angle-ply simply supported (SSSS) plate: a) fundamental frequencies and b) fundamental loss factors.

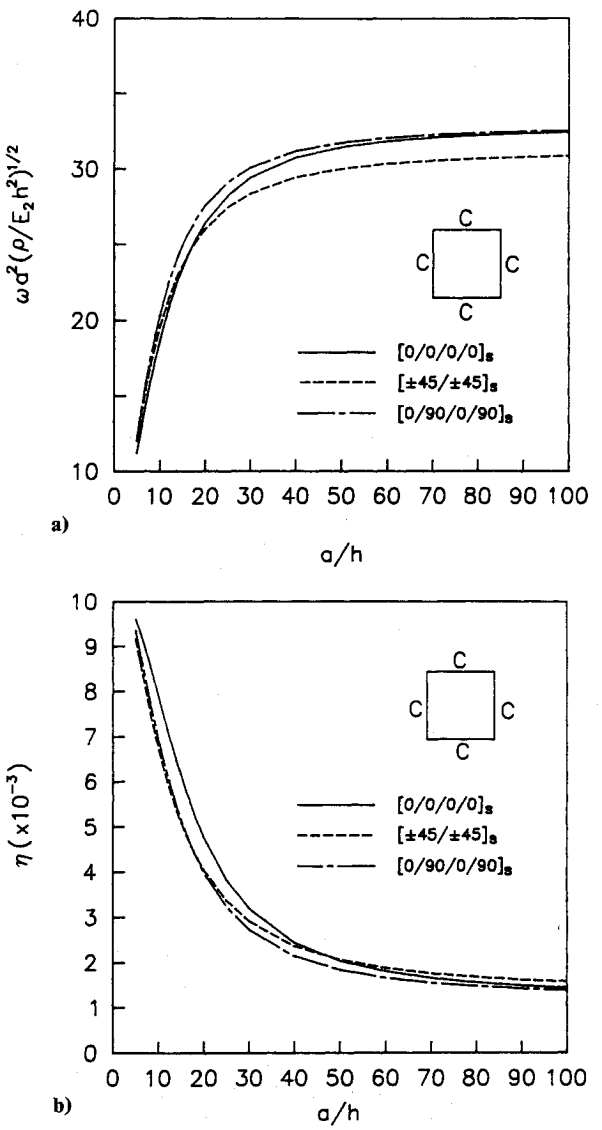

Fig. 6 Fundamental frequencies and loss factors for unidirectional, cross-ply, and angle-ply clamped (CCCC) plate: a) fundamental frequencies and b) fundamental loss factors.

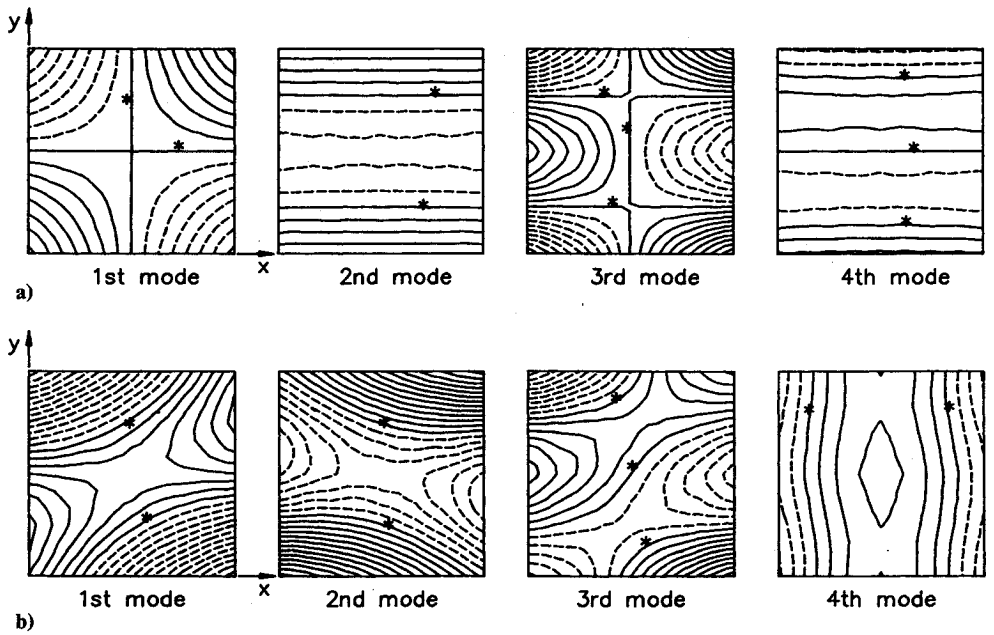

Fig. 7 Contour plots for $[0/\pm\theta/90]_s$ laminate (* denotes nodal line: a) $\theta = 0$ deg and b) $\theta = 45$ deg.

is 45 deg, the mode shapes are quite different from those for the zero fiber orientation.

Figures 8–11 show the natural frequencies and the modal loss factors for the various fiber orientations. Figure 8 shows the natural frequencies and the modal loss factors for the first mode of which the typical shape is pure torsion related with in-plane shear at $\theta = 0$ and 90 deg. The plates for the fiber orientation besides $\theta = 0$ and 90 deg have less damping by virtue of bending-torsion coupling. When the fiber orientation is near 45 deg, the natural frequency becomes the highest value and the loss factor becomes the lowest value. Figure 9 shows the natural frequencies and the modal loss factors for the second mode of which the typical shape is the first bending. When θ is zero, the second mode shape is pure bending.The reason for the higher value of the modal loss factors in the range of $\theta = 0$–20 deg is that a large amount of energy dissipation occurs in the matrix. As the fiber orientation increases, the fibers in the $\pm\theta$ layers retain higher strain energy to increase the natural frequency and decrease the modal loss factor. Figure 10 shows the results of the third mode of which the shape is the second torsion. When the fiber orientation θ is 0 deg, the torsional deformation results in a large amount of matrix deformation in $\pm\theta$ layers. Therefore, the natural frequency is the lowest and the modal loss factor is the highest at $\theta = 0$ deg. Figure 11 depicts the results for the fourth mode. The severe change in mode shape occurs in the fiber orientation between 35 and 40 deg. At this fiber orientation, the modal transfer will occur. This phenomenon can be explained by the curve veering phenomena.[14,15] The fourth mode is a bending dominant mode.

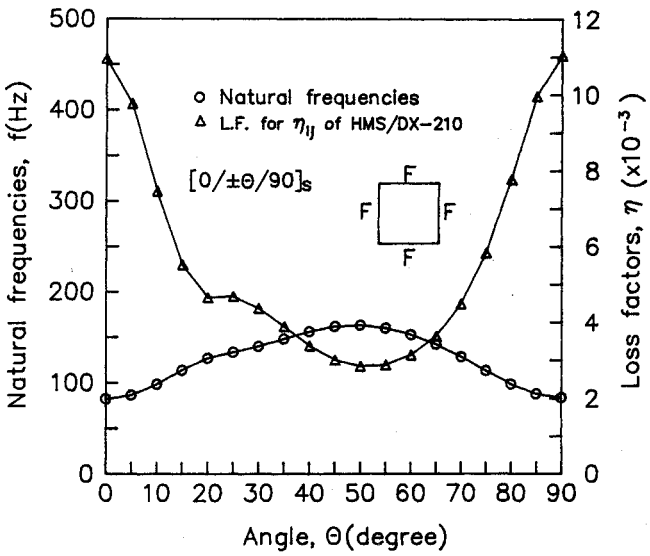

Fig. 8 Natural frequencies and modal loss factors of the first mode for the $[0/\pm\theta/90]_s$ plate.

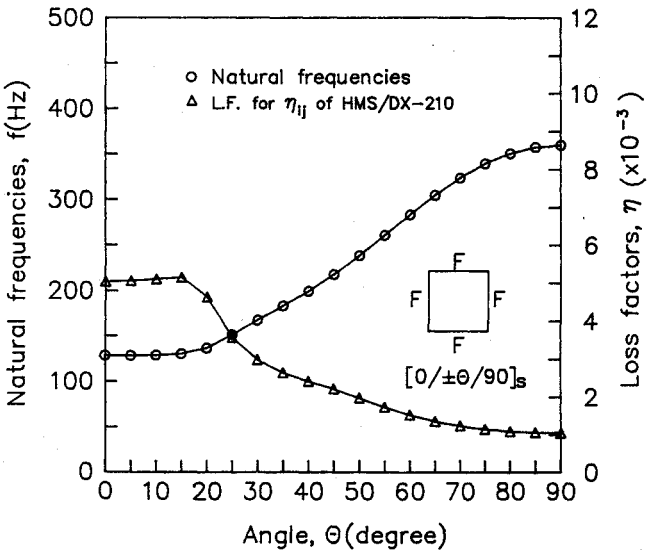

Fig. 9 Natural frequencies and modal loss factors of the second mode for the $[0/\pm\theta/90]_s$ plate.

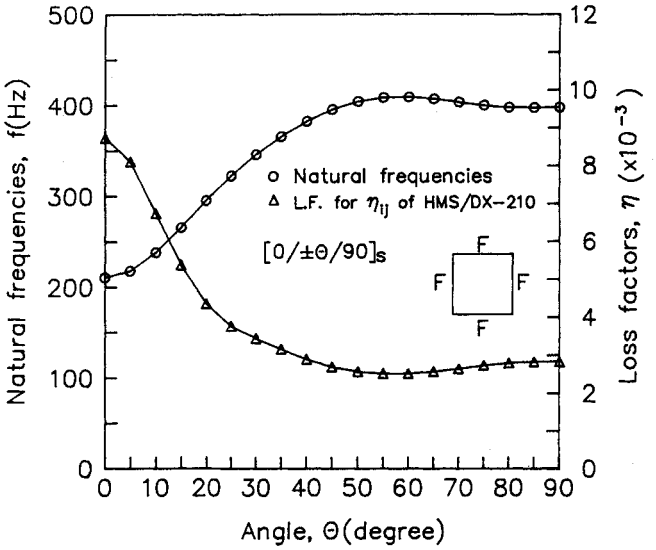

Fig. 10 Natural frequencies and modal loss factors of the third mode for the $[0/\pm\theta/90]_s$ plate.

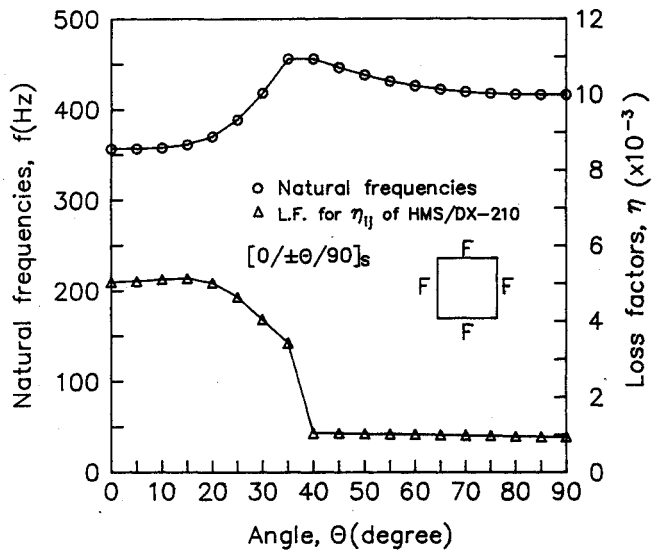

Fig. 11 Natural frequencies and modal loss factors of the fourth mode for the $[0/\pm\theta/90]_s$ plate.

Conclusions

The shear deformable plate theory is applied to the vibration and damping analysis of the fiber-reinforced composite laminated plates. The complex eigenvalue problem using finite element method is solved by the modal approach, which gives accurate results and saves a large amount of computation time.

The effects of the transverse shear on the natural frequencies and the modal loss factors are studied for the various boundary conditions and stacking sequences. The result shows that the transverse shear effect of the composite laminated plates gives high damping. Boundary condition affects the damping as well as natural frequency. Among the clamped,

simply supported, and free plates, the clamped plate has the highest transverse shear effect, and the transverse shear effect increases as the mode number increases.

Also, the effects of the fiber orientation on the natural frequencies and the modal loss factors are investigated for thin plates. The modal loss factor is greatly affected by the mode shape and is large when the matrix is subjected to the torsional shear deformations. Therefore, both the transverse shear and the in-plane shear increase the value of the damping of the composite plate.

References

[1]Bert, C. W., "Composite Materials: A Survey of the Damping Capacity of Fiber Reinforced Composites," *Damping Applications for Vibration Control*, AMD-Vol. 38, American Society of Mechanical Engineers, New York, 1980, pp. 53–63.

[2]Mallick, P. K., *Fiber-Reinforced Composites: Materials, Manufacturing, and Design*, Marcel Decker, Inc., New York, 1988, pp. 265–266.

[3]Gibson, R. F., and Plunkett, R., "Dynamic Stiffness and Damping of Fiber-Reinforced Composite Materials," *Shock and Vibration Digest*, Vol. 9, No. 2, 1977, pp. 9–17.

[4]Lin, D. X., Ni, R. G., and Adams, R. D., "Prediction and Measurement of the Vibration Damping Parameters of Carbon Glass Fiber-Reinforced Plastics Plates," *Journal of Composite Materials*, Vol. 18, March 1984, pp. 132–152.

[5]Bicos, A. S., and Springer, G. S., "Analysis of Free Damped Vibration of Laminated Composite Plates and Shells," *International Journal of Solids and Structures*, Vol. 25, No. 2, 1989, pp. 129–149.

[6]Hashin, Z., "Complex Moduli of Viscoelastic Composites—II. Fiber Reinforced Materials," *International Journal of Solids and Structures*, Vol. 6, No. 6, 1970, pp. 797–807.

[7]Alam, N., and Asnani, N. T., "Vibration and Damping Analysis of Fiber Reinforced Composite Material Plates," *Journal of Composite Materials*, Vol. 20, June 1986, pp. 2–18.

[8]Malhotra, S. K., Ganesan, N., and Veluswami, M. A., "Vibration and Damping Analysis of Orthotropic Triangular Plates," *Journal of Sound and Vibration*, Vol. 130, No. 3, 1989, pp. 379–386.

[9]Edberg, D. L., "Measurement of Material Damping in a Simulated Space Environment," Ph.D. Thesis, Dept. of Aeronautics and Astronautics, Stanford Univ., Stanford, CA, 1984.

[10]Yang, P. C., Norris, C. H., and Stavsky, Y., "Elastic Wave Propagations in Heterogeneous Plates," *International Journal of Solids and Structures*, Vol. 2, No. 4, 1966, pp. 665–684.

[11]Vinson, J. R., and Sierakowski, R. L., *The Behavior of Structures Composed of Composite Materials*, Martinus Nijhoff, Dordrecht, The Netherlands, 1987, pp. 54, 55.

[12]Reddy, J. N., *An Introduction to the Finite Element Method*, McGraw-Hill, New York, 1984, pp. 296, 297.

[13]Saravanos, D. A., and Chamis, C. C., "Unified Micromechanics of Damping for Unidirectional and Off-Axis Fiber Composite," *Journal of Composite Technology and Research*, Vol. 12, No. 1, 1990, pp. 31–40.

[14]Perkins, N. C., and Mote, C. D., Jr., "Comments on Curve Veering in Eigenvalue Problems," *Journal of Sound and Vibration*, Vol. 106, No. 3, 1986, pp. 451–463.

[15]Lee, I., and Lee, J. J., "Vibration Analysis of Composite Plate Wing," *Computers and Structures*, Vol. 37, No. 6, 1990, pp. 1077–1085.